SUBMARINE UNDERWATER STRUCTURE-BORNE NOISE AND FLOW NOISE DUE TO PROPELLER EXCITATION

Yingsan Wei, Yongsheng Wang, Ke Ding and Jian Fu
Department of Mechanical Engineering, Naval University of Engineering, Wuhan, PR China
weiyingsan@163.com

The current study presents the numerical prediction of the noise and vibration of a small-scaled submarine under axial excitation from a 5-bladed propeller and excitation from the flow noise induced by the pulsating pressure of the hull. Firstly, the propeller flow and submarine flow were independently validated. The propulsion of the hull-propeller was simulated using computational fluid dynamics (CFD), so as to obtain the transient responses of the propeller axial excitation and the boundary pressure of the hull. Finally, the acoustic response of the submarine under axial excitation was predicted using a finite element/boundary element model in the frequency domain, and the flow noise was predicted using Curle's analogy in the time domain.

INTRODUCTION

Propeller excitation can induce strong submarine vibration and radiated underwater noise [1,2]. As the propeller is operating in a spatially non-uniform wake of the submarine, the propeller thrust and boundary pressure of the submarine hull are fluctuating, which can generate significant acoustic signature [3]. Early research shows that the sound radiation transmitted through fluid is only 6-8% of that transmitted through shaft, while recent results show that this ratio is between 10-50% [4]. In most studies on submarine noise due to propeller excitation, the propeller excitation is assumed to have constant unit strength [4,5], and the pressure field in the fluid due to the propeller is represented by the fields due to dipoles in different directions at the propeller centre [6]. Merz [7] noted that the combination of CFD and finite element/boundary element (FE/BE) models are the trend for future studies of the propeller induced submarine hull vibration and underwater noise radiation.

In the current work, the propeller excitation and the boundary flow of the hull are simulated via CFD. The structure-borne noise and flow noise of the submarine are predicted using the BEM and Curle's analogy, respectively. The hydrodynamic fields of the submarine and propeller are simulated using CFX commercial software. The frequency response function of the submarine is simulated using ANSYS commercial software and an in-house code is developed to solve the acoustic response. The following assumptions are used: (1) only the axial excitation of the propeller transmitted from the shaft to the hull is considered, and the hull excitation via the fluid is ignored; (2) flow noise associated with fluctuating surface pressures on the propeller blades is not included in the current work; (3) the damping effect of the material is neglected; and (4) the excitations of the propeller are taken as concentrated point forces, not the distributed force on the blade.

ANALYTICAL MODEL

Boundary integral equation for acoustic problem

In a homogeneous medium, for the 3D linear time-harmonic problem for external acoustics using the Neumann boundary condition, the Helmholtz equation is

$$\Delta p(\mathbf{x}) + k^2 p(\mathbf{x}) = 0\ ,\ \ \mathbf{x} \in D \tag{1}$$

The solution can be obtained using the Burton-Miller formulation [8]

$$\int_s \frac{\partial G(\mathbf{x},\mathbf{y})}{\partial n(\mathbf{y})} p(\mathbf{y}) dS(\mathbf{y}) + C(\mathbf{x}) p(\mathbf{x}) + \alpha \int_s \frac{\partial^2 G(\mathbf{x},\mathbf{y})}{\partial n(\mathbf{y}) \partial n(\mathbf{x})} p(\mathbf{y}) dS(\mathbf{y})$$

$$= \int_s G(\mathbf{x},\mathbf{y}) q(\mathbf{y}) dS(\mathbf{y}) + \alpha \int_s \frac{\partial G(\mathbf{x},\mathbf{y})}{\partial n(\mathbf{x})} q(\mathbf{y}) dS(\mathbf{y}) - C(\mathbf{x}) q(\mathbf{x}),\ \mathbf{x} \in \partial D \tag{2}$$

where $\mathbf{x}$ is a general field point, $\mathbf{y}$ is the source point, p is the acoustic pressure, $n(\mathbf{y})$ is the unit normal at $\mathbf{y} \in \partial D$, D is the domain of the propagation, ∂D is the boundary of D, $v_n(\mathbf{x})$ is the normal velocity, $C(\mathbf{x})$ is a geometry related coefficient, $G(r) = -e^{ikr}/4\pi r$ is the free space Green's function, with $r = ||\mathbf{x}-\mathbf{y}||_2$, α is the coupling constant, q is the derivative of p. Once the sound pressure on the boundary is known, the pressure at any point in the exterior field can be determined by

$$C(\mathbf{x}_i)\, p(\mathbf{x}_i) = \int_s G(\mathbf{x}_i,\mathbf{y}) q(\mathbf{y}) - p(\mathbf{y}) \frac{\partial G(\mathbf{x}_i,\mathbf{y})}{\partial n(\mathbf{y})} dS(\mathbf{y}),\ \ \mathbf{x}_i \in \partial D \tag{3}$$

Curle's analogy for pulsating pressure induced flow noise

In the time domain, the flow noise induced by the pulsating pressure on the solid boundary can be obtained via Curle's analogy [9]

$$p(\mathbf{r},t) = \int_s [\mathbf{n}\cdot\mathbf{r} \,/\, (4\pi c r^2) * (\partial p_s \,/\, \partial t)\ ]_\tau\, dS \tag{4}$$

where c is the speed of sound in the fluid and p_s is the boundary pressure. As the submarine is not acoustically compact, (i.e. $\omega L/c$~1.0, with L being the submarine length), the time derivative of the pressure is calculated at the retarded time τ. In Eq. (4), the volume source is neglected, because the noise contribution from the flow field surrounding the body is included in the quadrupole sources which is relatively small compared to the term in Eq. (4).

HYDRODYNAMIC AND ACOUSTIC CHARACTERISTICS OF THE HULL-PROPELLER

In this work, a five bladed unskewed propeller model as shown in Table 1 is chosen to match the SUBOFF submarine for two reasons. (1) Firstly, the test data of the propeller and the experimental data of the submarine can validate the numerical results. (2) Secondly, in Ref. [10], the aforementioned propeller was used to thrust a standard axisymmetric submarine hull model (DTMB model 5495-3) in the US Navy's LCC. The parameter values of the SUBOFF submarine are listed in Table 2, and the sail is located on the hull at the top dead centre. The stern appendages are attached to the hull at ϕ=0°, 90°, 180° and 270°, where ϕ is defined positive counter-clockwise as viewed from the stern. Experimental data of the SUBOFF for validation was provided by David Taylor Model Basin (DTMB) in 1988 and 1989 [11]. A number of submarine configurations, ranging from an axisymmetric body to a fully appended submarine were constructed in order to provide flow measurements for the CFD validation. Each model was placed in the Anechoic Flow Facility (AFF) wind tunnel. The flow was measured at a Reynolds number of 1.2×10^7. In the experiment, pressure taps on the hull surface connected to rotary pressure scanners provided measurements for surface pressure. A traversing mechanism was used to position hot film probes in order to measure mean axial components of the velocity profile at non-dimensionalised positions of X/L=0.978, where X is the position along the hull.

Table 1. Parameter values of the propeller

Diameter	Number of blades	Hub-to-diameter ratio	Expanded area ratio	Blade section	Design advance coefficient	skew	rake
0.25m	5	0.2	0.725	NACA66 (modified)	0.889	0	0

Table 2. Parameter values of the submarine

Submarine length L	Maximum diameter D_s	Forebody length	Midbody length	Afterbody length	Appendages
4.36m	0.51m	1.02m	2.23m	1.11m	NACA0020

Hydrodynamics of independent propeller and independent submarine

Firstly the single passage of the propeller is meshed, with the local areas such as the tip and the root refined, as shown in Fig. 1. The total number of the single passage meshes is 0.38M, the y-plus value on the boundary of the blade is about 84, herein the y-plus value represents the non-dimensional distance of the first node from the wall, which is recommended in the scope of 20 to 100, and in this case the mixed formulation of wall function (i.e. automatic near wall treatment in CFX) is selected. This mixed method is available for all frequency equations based turbulence models, which automatically switch from a low-Reynolds number formulation to wall functions based on the grid spacing provided by the user. The mixed formulation provides the optimal boundary condition for a given grid. The calculation domain of the independent propeller is shown in Fig. 2. The propeller angular speed is 650rpm in this section, and the propeller rotates anti-clockwise, looking forward through the propeller disc. Here, the advance ratio of the propeller changes from 0.1 to 1. For the computational models the inlet boundary conditions consists of the prescribed velocity profile. At the outlet $p_{ave}=p_0$ and $(\nabla\mathbf{v}).\mathbf{n}=0$ and no-slip conditions are used on the blades. Finally the thrust coefficient K_t, the torque coefficient K_q, and the open water efficiency η can be determined via CFD, with $K_t=T/(\rho N_p^2 D^4)$, $K_q=Q/(\rho N_p^2 D^5)$, $\eta=(J/2\pi)K_t/K_q$, where T, Q ,N_p, D are respectively the blade thrust, torque, rotating speed and diameter. The numerical model is based on the Reynolds Averaged Navier-Stokes (RANS) equations, with the body forces due to the blade's rotation being treated based on the quasi-steady Multiple-Frame-of-Reference method. The turbulent flow within the blade is formulated in a rotating reference frame, the Shear Stress Transport (SST) turbulent model is adopted in this paper [12]. As shown in Fig. 3, the K_t, K_q values of the propeller agree well with the experimental results, whilst the open water efficiency η slightly differs.

For the hydrodynamic field of the submarine independently from the propeller, a circular computational domain is used. The computational domain size is set according to Ref. [11]. The domain extends one hull length upstream of the submarine model and two hull lengths downstream of the model, thus being 4L in overall length. The outer diameter of the cylinder is $10D_s$. The inflow velocity is V_s=3.036m/s and the SST turbulent model is adopted. The inlet boundary condition consists of the prescribed velocity profile. At the outlet $p_{ave}=p_0$ and on the hull $(\nabla\mathbf{v}).\mathbf{n}=0$. No-slip conditions are used. The far-field boundary conditions are used at the circumferential boundaries of the

computational domains, as described in Ref [11]. To capture the flow detail on the hull and appendages, the meshes near the boundary, the sail and the rudders are refined. From a mesh independent analysis, when the total mesh number reaches 2.06M, the resistance of the submarine converges at 100.2N, with 2.05% relative error compared with the experiment. To further validate the accuracy of the submarine flow, the static pressure coefficients C_p along the meridian line of the hull, at 50% of stern appendage-tip chord length, and at 10% of sail-tip chord length are compared with the experimental results from Ref. [11] in Fig. 4, with $C_p=(p-p_0)/(0.5\rho V_s^2)$, where p is the local static pressure and p_0 is the ambient pressure. Thereafter, the axial non-dimensional velocity with the reference velocity being V_s at streamwise of X/L=0.978 is also validated, as shown in Fig. 5. The contour changes from the range of a minimum value of 0.45 to a maximum of 0.9 with an increment of 0.05, and shows good agreement.

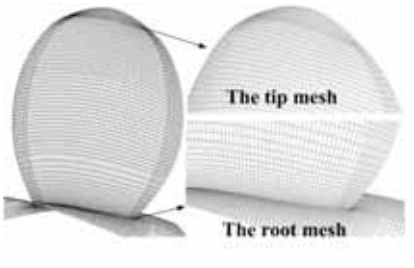

Figure 1. Meshes of the propeller

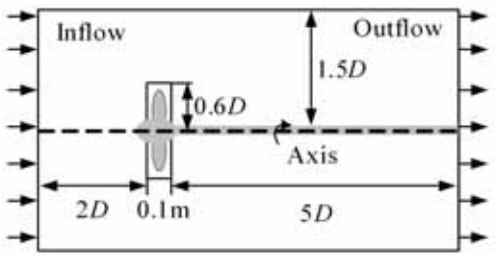

Figure 2. Calculation domain of the propeller

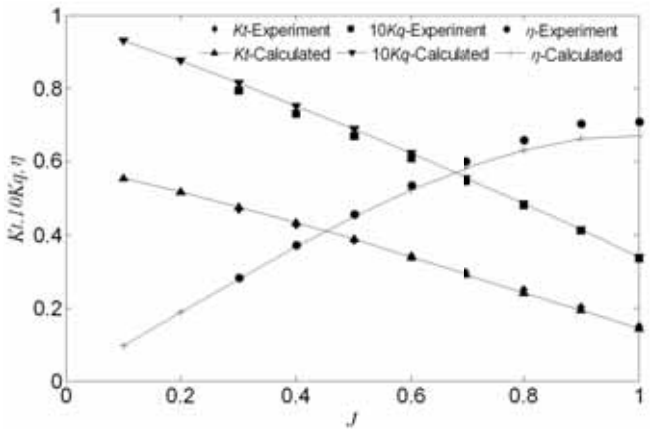

Figure 3. Open water characteristic of the propeller

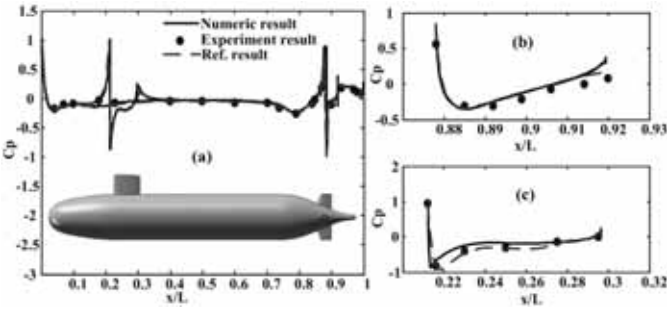

Figure 4. C_p comparison (a) C_p along the meridian line of the hull, (b) C_p at 50% of stern appendage-tip chord length, (c) C_p at 10% of sail-tip chord length

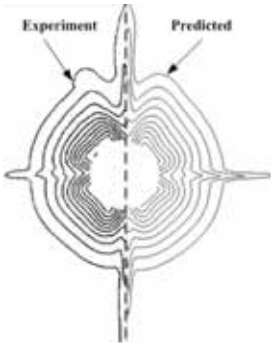

Figure 5. Axial component velocity profile at X/L=0.978

Hydrodynamics of hull-propeller system

As the independent flow of the propeller and submarine is validated, the propeller and submarine are now combined to determine the steady-state responses. The total meshes of the system are shown in Fig. 6, with the global number of nodes and elements 4.13M and 3.97M, respectively. The y-plus value is about 80, and the automatic near wall treatment is adopted. Firstly a steady flow of the system is simulated via CFD, with the advection term and the momentum equation discretized by the second order upwind scheme. Changes in the propeller rotation speed (N_p), the propeller thrust (T), and the submarine resistance (R) allow the operating point to be determined at the chosen inflow velocity of V_s=3.036m/s, as shown in Fig. 7. The steady-state response is then determined at the intersection of the two curves (T~N_p and R~N_p). The parameter values of the hull-propeller at the steady-state are listed in Table 3. Under such circumstances, the propulsion factors such as the propeller advance ratio J, the wake fraction w, and the thrust deduction t, can be determined and respectively correspond to J=0.849, w=0.225 and t=0.202.

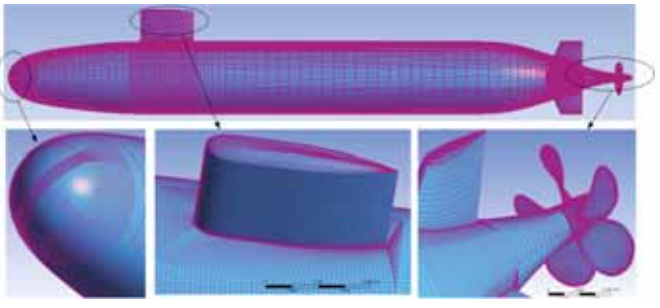

Figure 6. Meshes of the hull and propeller

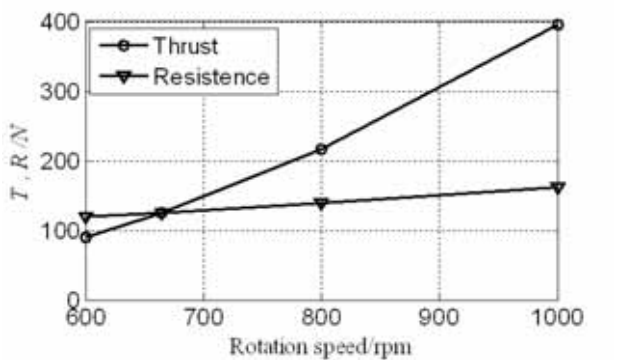

Figure 7. Propeller thrust (T) and submarine resistance (R) versus propeller rotation speed (N_p)

Table 3. Parameter values of the hull-propeller at steady-state

Inflow velocity	Propeller speed	Thrust	Resistance
3.036m/s	665rpm	125.82N	125.57N

Taking the steady flow result as the initial condition of the transient flow calculation, the propeller axial force and the pulsating pressure of hull are obtained. In the transient analysis, the meshes of the propeller are physically rotated, and the time step is 0.001s with a total simulation time of 10s. The SST turbulent model is adopted with the advection term. The momentum equation is discretized by the second order upwind scheme. The transient formulation is solved by the second order implicit scheme. Then the propeller thrust is obtained by integrating the pressure on the blade surface

$$T = \int_S p n_x dS \tag{5}$$

Figure 8 shows the propeller thrust and monitor pressure in front of the propeller. Both are tonal at the propeller harmonics in the frequency range up to 500Hz.

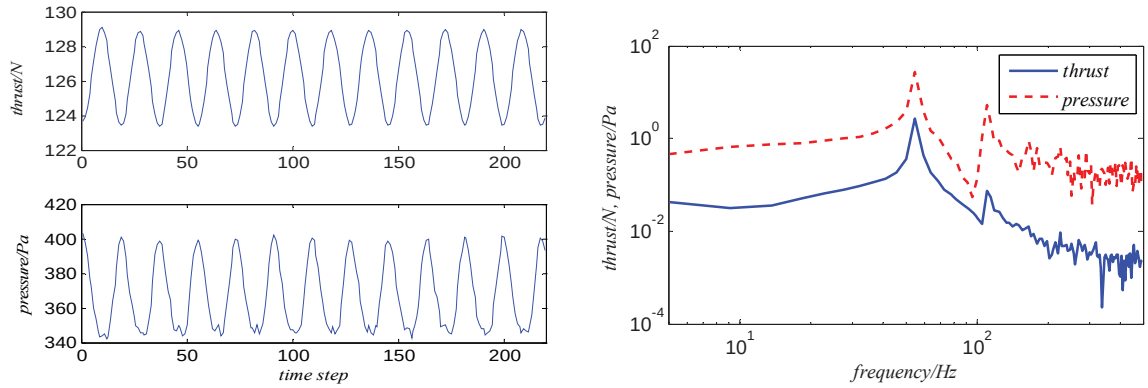

Figure 8. Fluctuations of the thrust and pressure in the time domain (left) and in the frequency spectrum (right)

Acoustic response analysis

In this section, the structure-borne noise and the flow noise of the submarine are predicted. Firstly, the finite element model of the submarine is built, as shown in Fig. 9. The structure is divided into five compartments by four bulkheads with ring stiffeners and longitudinal rib stiffeners, as shown in Fig. 9(b). To ensure the local intensity of the sail and "+" typed rudders, the appendages are also stiffened. The hull and bulkheads are represented by 26,739 SHELL63 elements, and the ribs by 5,517 BEAM188 elements. The SHELL63 is a type of elastic element with 6 degrees of freedom (DOF) which is always used to model both in-plane and out-of-plane vibration of a thin plate. The BEAM188 is a type of line element with 6 DOF which is suitable for analysing slender to moderately thick beam structures. The thickness of the hull and the bulkheads is 6mm. The rib section on the hull is of an inverted T shape, and the rib section on the appendage is of an H shape, as shown in Figs. 9(c) and (d), respectively. The material of the submarine is steel, and the structural loss factor is ignored. Considering the fluid-structure interaction, the surrounding fluid of the submarine hull is also modelled to couple the pressure and structural velocity on the boundary nodes. The axial excitation is then loaded on the bulkhead centre of the cabin near the stern, as shown in Fig. 9(a), and the structural response of the hull is calculated. Here, the shaft and the bearing dynamics are not considered in the FE model. The normal velocity of the hull was used as the boundary condition of the boundary element (BE) model. The finite elements of the hull were directly used as the boundary elements to ensure the coincidence of the FE/BE models, with no error of the data projection introduced. In this work, FEM and BEM are separately used. The fluid-structure interaction effect is modelled by FLUID30 element in FEM, which differs from the method in Ref. [7].

To predict the flow noise, the pressure and the geometry information of the submarine should be known. Here, the boundary pressure of the hull at each time step, the area, and the normal vector are exported from CFD. Finally, the sound pressure is predicted using Eq. (4) in the time domain and the flow noise is transformed to the frequency spectrum using FFT. Thereafter the structure-borne noise and flow noise of the submarine are evaluated at a field point P that is 10L downstream. The reference pressure is 1μPa and the frequency range is 0 to 500Hz. The result in Fig. 10 shows the presence of blade pass frequency (BPF) tonals at multiples of 55.4Hz in both the structure-borne noise and flow noise including

the effects of propeller rotation, while the effects of resonant hull responses to broadband random excitation can be seen at 238Hz and 400Hz. Flow noise including the effects of rotation falls with increasing frequency above around 350Hz. The frequency response function (FRF) of the normal displacement of the submarine shown in Fig. 11 shows the principal bending mode of the hull at 180Hz, the breathing mode at 238Hz, the resonant mode of the rudders at 371Hz and the circumferential mode of the cabins at 400Hz. As the field point is located at the end of the submarine, the breathing mode has a significant contribution to the sound pressure.

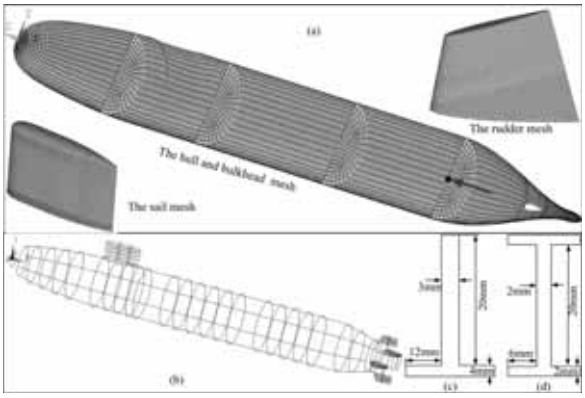

Figure 9. Finite element model of the submarine showing (a) shell elements, (b) beam elements, (c) ribs of an inverted T shape, (d) ribs of an H shape

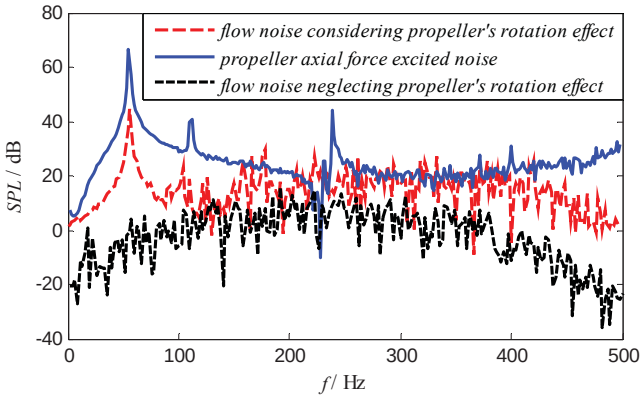

Figure 10. Submarine underwater noise at the field point P

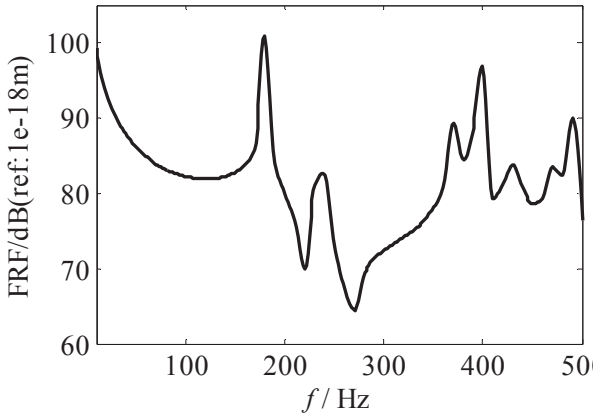

Figure 11. Frequency response of the normal displacement of the submarine under unity axial force

Figure 12 presents the time history of the flow noise considering the propeller rotating effect. A distinct fluctuation of the signature is observed. Figure 13 shows the maximum sound pressure level of the structure-borne noise and the flow noise in the horizontal plane at a distance of 10*L* from the submarine centre at the propeller harmonics. Figure 14(a) and 14(b) show the sound directivity of the two types of noise at the first harmonic of the propeller. The zero degree refers to the submarine stern part. In order to analyse the effect of the rotating propeller on the flow noise, the flow noise in the absence of the rotating propeller is also plotted in Fig. 10 and Fig. 14(c). Figure 14(c) represents the sound directivity of the flow noise at 354Hz when the propeller rotating effect is ignored. As shown in Fig. 10, at 354Hz the flow noise begins to fall. Results at the selected speed show that (1) the SPL of the structure-borne noise and flow noise differs by more than 20dB at BPF and by around 10dB at 2BPF. At 3BPF to 5BPF, the flow noise surpasses the structure-borne noise by 4dB to 10 dB. It can be concluded that the flow noise is about 10% of the structure-borne noise at propeller blade passing frequency. (2) The noise due to the axial force is mainly radiated from the conical end caps, while the noise due to the flow is mainly radiated from the cylindrical hull. As the axial force mainly excites the submarine axial mode (or breathing mode), the majority of the sound energy is radiated from the conical end caps. (3) Due to the rotating effect of the propeller, the directivity of the flow noise is asymmetric relative to the axis of the submarine. When the propeller rotates in the wake of the submarine, the boundary pressure of the hull is influenced by the propeller, and this represents the effect of rotating forces and volumes. To investigate this phenomenon, the flow noise is also calculated when propeller meshes are excluded in the flow field of the submarine, so that the boundary flow of the hull is not affected by the propeller. Under such conditions, the SPL of the flow noise is plotted in Fig. 10. The maximum SPL is about 20dB, and the sound directivity is symmetric relative to the vertical plane of the submarine as shown in Fig. 14(c), but with relatively small magnitude.

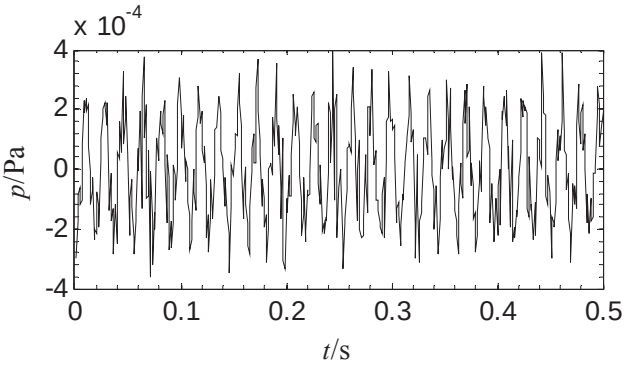

Figure 12. Time history of the flow noise

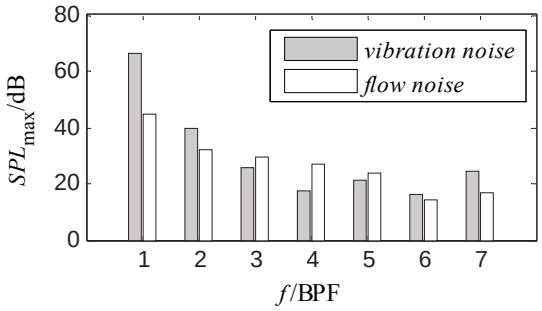

Figure 13. Maximum sound pressure level at propeller harmonics

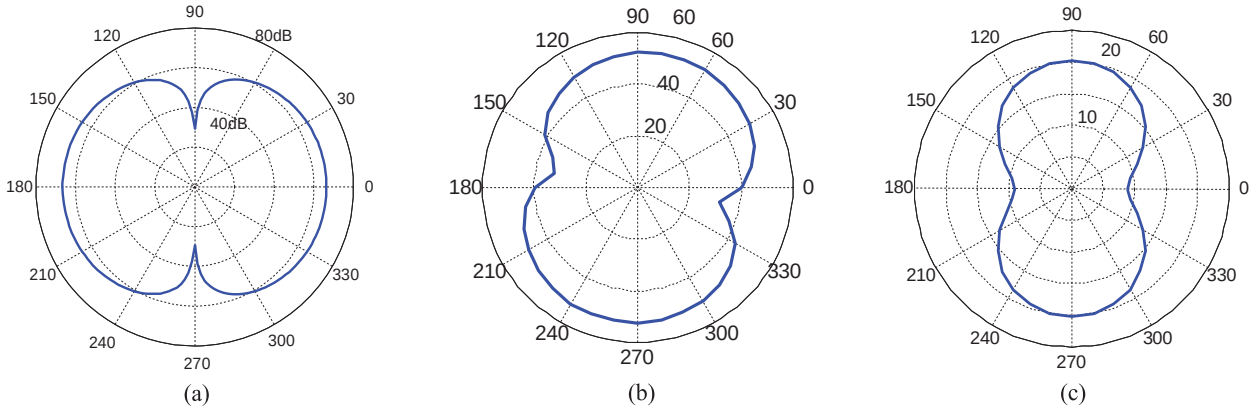

Figure 14. Sound directivity pattern in the horizontal plane at a distance 10L showing (a) structure-borne noise at BPF, (b) flow noise considering the rotating effect of the propeller at BPF, (c) flow noise ignoring the rotating effect of the propeller at 354Hz

CONCLUSIONS

This paper presents the structure-borne noise and flow noise of a submarine under axial excitation from a propeller running at low Reynolds number. The results have been derived for a specific set of model parameters with a small-scale model. In current work, only the flow noise associated with fluctuating surface pressure on the submarine hull is considered. Results show that (1) under axial excitation, the principal breathing and bending modes plus the resonance mode of the rudders and circumferential modes of the cabins generate strong structural responses. The resulting sound pressure at the field point is tonal at the propeller harmonics and structural resonances. (2) The flow noise occurs mainly around the propeller harmonics. (3) The noise due to the axial force is mainly radiated from the conical end caps, while the noise due to the flow is mainly radiated from the cylindrical hull. (4) The flow noise is lower than the structure-borne noise at the blade passing frequency (BPF), and higher than the structure-borne noise at higher harmonics of BPF. (5) Due to the propeller rotating effect, the directivity of the flow noise is asymmetric relative to the axis of the submarine.

REFERENCES

[1] M. Caresta, N.J. Kessissoglou and Y.K. Tso, "Low frequency structural and acoustic responses of a submarine hull", *Acoustics Australia* **36**(2), 47-52 (2008)

[2] Lu Shi-jin, Yu Meng-sa and Li Dong-sheng, "Prediction of hydrodynamic radiation noise of underwater vehicle", *Journal of Hydrodynamics* **22**(4), 475-482 (2007) (in Chinese)

[3] M. Caresta and N.J. Kessissoglou, "Acoustic signature of a submarine hull under harmonic excitation", *Applied Acoustics* **71**(1), 17-31 (2010)

[4] E. van Wijngaarden, "Recent developments in predicting propeller-induced hull pressure pulses", *Proceedings of the 1st International Ship Noise and Vibration Conference*, London, UK, 20-21 June 2005

[5] J. Brouwer, *Ship propeller-induced noise and vibrations - prediction and analysis*, M.Sc. Thesis, University of Twente, The Netherlands, 2005

[6] R. Kinns, I.R.M. Thompson, N.J. Kessissoglou and Y.K. Tso, "Hull vibratory forces transmitted via the fluid and the shaft from a submarine propeller", *Ships and Offshore Structures* **2**(2), 183-189 (2007)

[7] S. Merz, R. Kinns and N.J. Kessissoglou, "Structural and acoustic responses of a submarine hull due to propeller forces", *Journal of Sound and Vibration* **325**, 266-286 (2009)

[8] A.J. Burton and G.F. Miller, "The application of the integral equation methods to the numerical solution of some exterior boundary-value problems", *Proceedings of the Royal Society of London, Series A* **323**(1553), 201–210 (1971)

[9] N. Curle, "The influence of solid boundaries upon aerodynamic sound", *Proceedings of the Royal Society of London, Series A* **231**(1187), 505-514 (1955)

[10] D.H. Bridges, *A detailed study of the flowfield of a submarine propeller during a crashback maneuver*, Office of Naval Research Grant No. N00014-97-1-1069, Final Report, MSSU-ASE-04-1, 2004

[11] N. Alin, C. Fureby, U. Svennberg, W. Sandberg, R. Ramamuti, R. Bensow and T. Persson, "3D unsteady computations for submarine-like bodies", *Proceedings of the 43rd AIAA Aerospace Sciences Meeting and Exhibit*, Nevada, US, 10-13 January 2005

[12] ANSYS Inc., ANSYS CFX-Solver Modeling Guide, Aerodynamics noise analysis, 2006